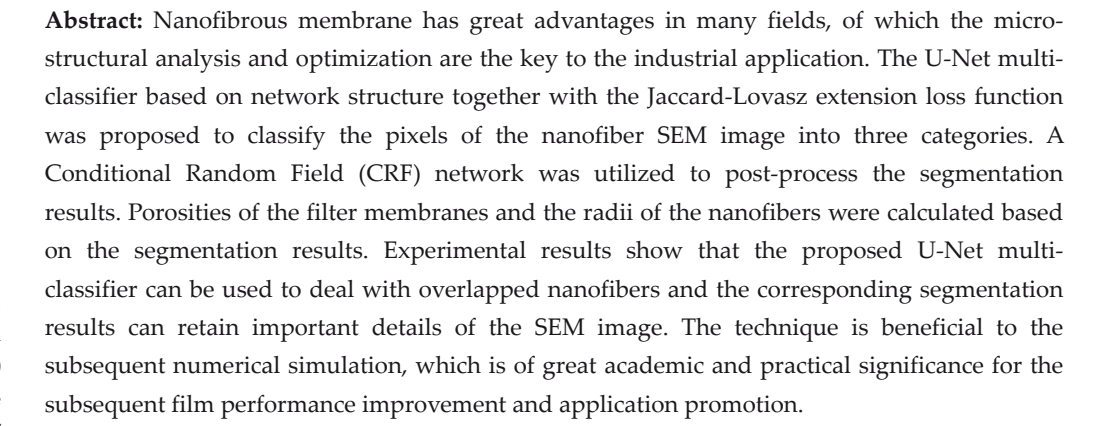


Article

## Feature Extraction of Nanofibers Based on U-Net Multi-classifier

Zebin Chen<sup>1</sup>, Meiqing Wang<sup>1</sup>, Fei Chen<sup>1</sup>, Shumin Guo<sup>2</sup>, Choi-Hong Lai<sup>3</sup>, Weiqi Gao<sup>4</sup>, Gaofeng Zheng<sup>4,5\*</sup>

- <sup>1</sup> School of Mathematics and Statistics, Fuzhou University, Fuzhou, Fujian, China
- <sup>2</sup> School of Mathematical Sciences, Xiamen University, Xiamen, Fujian, China
- <sup>3</sup> School of Computing and Mathematical Sciences, University of Greenwich, London, UK.
- <sup>4</sup> Pen-Tung Sah Institute of Micro-Nano Science and Technology, Xiamen University, Xiamen, Fujian, China
- <sup>5</sup> Shenzhen Research Institute of Xiamen University, Shenzhen, China
- \* Corresponding author email: zheng gf@xmu.edu.cn



Keywords: nanofiber SEM image segmentation; micro/nano technology; neural nets

© BY

Copyright: © 2025 by the authors. This article is licensed under a Creative Commons Attribution 4.0 International License (CC BY) license (https://creativecommons.org/licenses/by/4.0/).

Citation: Zebin Chen, Meiqing Wang, Fei Chen, Shumin Guo, Choi-Hong Lai, Weiqi Gao, Gaofeng Zheng. "Feature Extraction of Nanofibers Based on U-Net Multi-classifier." Instrumentation 12, no.3 (September 2025). https://doi.org/10.15878/j.instr.202500266

#### 1 Introduction

Nanofibrous filtration membranes, renowned for their economic feasibility and superior functional performance, have found wide-ranging applications in various fields<sup>[1,2]</sup>, including water pollution treatment<sup>[3]</sup>, air purification<sup>[4]</sup>, and medical wound dressings<sup>[5]</sup>. The market for nanofiber membrane applications has significantly expanded, with a promising outlook for future growth<sup>[6]</sup>. To cater to the escalating market demand for high-performance products, it is imperative to enhance the performance of nanofiber membranes. Optimizing the microstructure of nanofiber membranes is a key method to improve their functions. Research conducted by Chu et al. [7] on electrospun fibers of diverse patterns shows how fiber arrangement influences filtration efficiency and overall performance. Similarly, Pujiarti et al.<sup>[8]</sup> increased the porosity of fiber membranes by applying ACB to PAN substrates, effectively

enhancing their ability to store electrolytes. In recent years, the identification and analysis of microstructural characteristic parameters in fiber filtration membranes have effectively enhanced filtration performance and facilitated their specialized adaptation to the filtration needs of various industries<sup>[9,10]</sup>.

Scanning Electron Microscopy (SEM) has become a key method for closely examining the tiny and intricate structures of nanofiber membranes. Qu et al. [11] introduced microscopic optical materials and developed an innovative SEM-based operating system that can characterize various features of individual fibers. Lu et al. [12] used SEM and XRD to study fibers, exploring how process parameters affect their shapes. Their work shows the link between manufacturing conditions and fiber structures, highlighting the importance of these techniques in fiber analysis. Despite these advancements, extracting and analyzing structural characteristic parameters, such as fiber diameter and pore size within nanofiber filtration membranes, remains fraught with challenges. First, the dimensions involved are at the nanoscale, much smaller than even a single bacterium, and are typically discernible only through SEM imaging, which precludes direct measurement. Secondly, the precision of feature extraction is compromised by the inherent limitation of two-dimensional SEM images to delineate the layered stacking of nanofiber membranes. Third, nanofiber membranes, composed of randomly stacked individual fibers, exhibit an intricate micro and nano topological structure that challenges traditional image processing techniques in analyzing complex random structures<sup>[13]</sup>. Therefore, segmenting SEM images and extract their topological structure characteristic parameters remains a significant challenge in the analysis and optimization process.

With the advancement of artificial intelligence technology, neural network algorithms have shown promising results in image recognition and processing. FCN<sup>[14]</sup>, R-CNN<sup>[15]</sup>, MASK R-CNN<sup>[16]</sup>, and U-Net<sup>[17]</sup> are commonly used neural networks for image segmentation. U-Net excels at images by leveraging its U-shaped symmetric structure and skip connections to preserve fine structural details, while requiring fewer training samples, making it more adaptable to the limited SEM datasets commonly encountered in materials science. Ronneberger et al. introduced the U-Net neural network, which classifies SEM images of biological cells into foreground and background based on feature image information, achieving effective processing results. In this work, this method was applied to process SEM images of nanofiber filtration membranes. However, the standard U-Net, functioning as a binary classifier, showed poor performance when segmenting images with overlapping fibers, requiring optimization based on the characteristics of the fiber membranes.

This paper introduces an advanced multiclass classifier that combines the Jaccard-Lovász extension loss function<sup>[18]</sup> with the U-Net architecture for segmenting SEM images of nanofibers into foreground, mid-background, and background. After segmentation, a conditional random field was used to post-process the U-Net segmentation results to reduce boundary blurring. Additionally, the segmentation results were used to calculate the characteristic radius of nanofibers and the porosity of air filtration membranes, further validating the effectiveness of the image processing results. Numerical experiments indicate that the SEM image segmentation results obtained using the U-Net multi-classifier better preserve the topological information of fibers and yield more accurate characteristic parameters, providing more reliable technical support for analyzing the structure of fiber membranes.

#### 2 The U-Net Structure

The U-Net neural network, proposed by Ronneberger

et al. in 2015, adopts a symmetric encoder-decoder framework<sup>[19]</sup>, as depicted in Fig. 1. The encoder part consists of four blue NE nodes, denoted as NE1, NE2, NE3, and NE4, and four edges between the NE nodes denoted as  $\varphi_1$ ,  $\varphi_2$ ,  $\varphi_3$  and  $\varphi_4$ . Each NE node encapsulates a pair of "convolution + activation" operations; and each edge  $\varphi_i$  represents one downsampling operation.

The decoder is the inverse process of the encoder, including four green ND nodes, denoted as ND1, ND2, ND3, and ND4, and four edges between ND nodes, denoted as  $\psi_1$ ,  $\psi_2$ ,  $\psi_3$  and  $\psi_4$ . Each ND node also signifies a pair of "inverse convolution + activation" operations; and each edge  $\psi_i$  represents one upsampling operation.

In U-Net network, the ReLU function is used as the activation function. It is defined as the positive part of the argument and implemented via software computation.

The input image comes through NE1 node, performing double "convolution + activation" operations before converting to the feature map S which forms the argument of the downsampling operation  $\varphi_1$  and an input of ND1. The output of  $\varphi_1$  is the input of the NE2 node. The same process is performed through NE2 to NE4 nodes.

In the decoder part, through ND4 to ND2 process, ND1 node receives two inputs: the output of the upsampling operation  $\psi_1$  and S, the output of the NE1; performs double "inverse convolution + activation", output the feature map L (the label map) and F (the confidence map) which are the outputs of the whole U-Net.

As an example, Fig. 1(b) shows an enlarged structure of the NE1 node, where I is an input image,  $\xi_i$ ,  $i = 1, \dots, 64$ , are the intermediate feature maps; the vector of feature maps  $S = (S_1, \dots, S_{64})$  are the output of

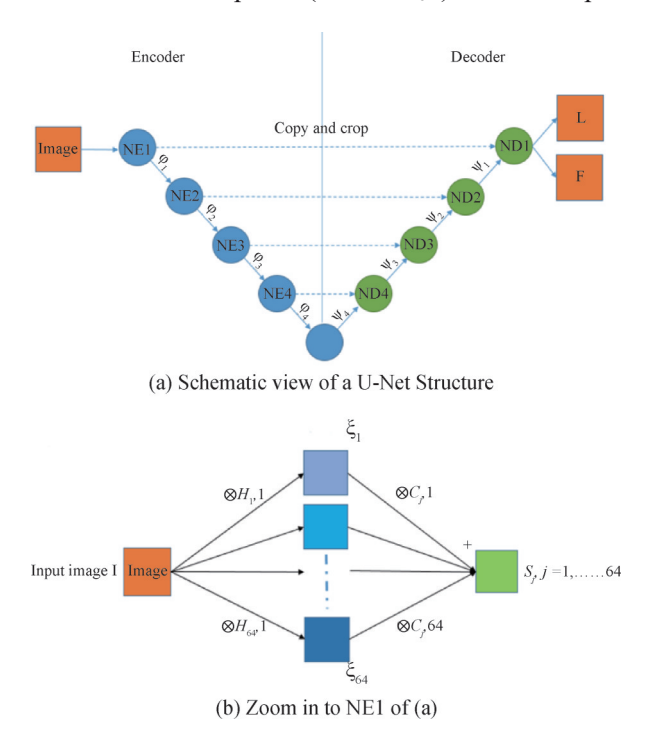


Fig.1 The U-Net Neural Network: (a) Schematic view of a U-Net Structure (b) Zoom in to NE1 of (a)

the NE1 node;  $h_{i1}$ ,  $i = 1, \dots, 64$ , and  $c_{ii}$ ,  $i, j = 1, \dots, 64$ , are the convolution kernels. Each convolution is followed by a ReLU unit, which is not shown in the figure. The calculation can be expressed as following formulae:

$$\xi_i = \sigma(I \otimes h_{i1}), \ i = 1, \dots, 64 \tag{1}$$

$$S_j = \sigma\left(\sum_{i=1}^{64} \xi_i \otimes c_{ji}\right), j = 1, \dots, 64$$
 (2)

where  $\sigma$  stands for the ReLU unit.

#### Nanofiber SEM Image Multi-3 classifier

#### 3.1 The Network Structure

The U-Net network was used to obtain some good

results in biomedical SEM image segmentation<sup>[17]</sup>. However, the U-Net network uses multiple downsampling operations, which leads to loss of some information. When this network is used to segment fiber SEM images, the target boundaries become blurred, and there are noise points inside the target (Fig. 3 (b)), which will affect the subsequent computational processes. In order to improve the accuracy of segmentation, a CRF (Conditional Random Field) module was used to post-process the prediction map output of the U-Net Network and finetune the boundary of the target objects in this paper.

The network structure is shown in Fig. 2. The fractions 1, 1/2, 1/4, 1/8 and 1/16 as seen in the U-Net module represent the downsampling and upsampling factors of each layer respectively.

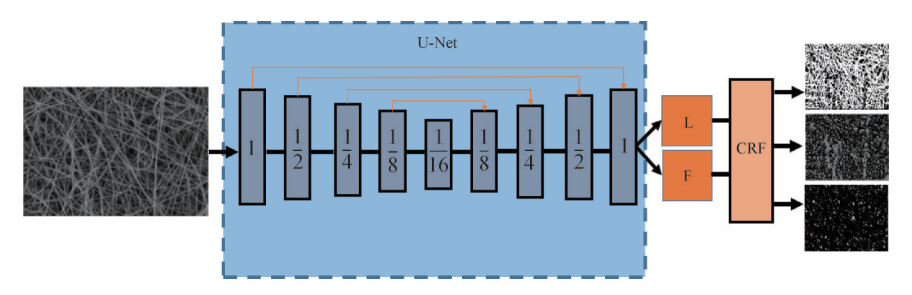


Fig.2 Network structure diagram

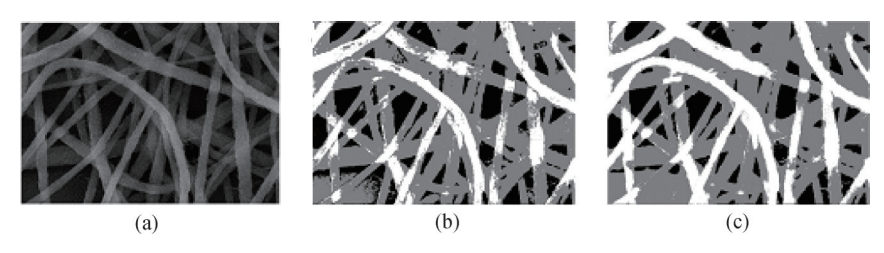


Fig. 3 A SEM image and its segmentation results: (a) SEM original image; (b) U-Net segmentation; (c) CRF post-processing

#### 3.2 Loss Function

The standard U-Net network uses a cross-entropy loss function as the measurement of classification accuracy. However, early tests demonstrated that the cross-entropy loss function does not work well with the validation dataset. Therefore, the multi-classification Jaccard-Lovasz extension loss function<sup>[20]</sup>, was used in this paper. This function is the Lovasz extension of the evaluation indicator Jaccard Index and is also known as intersection-over-union (IoU).

A training image with a size of  $\eta = H \times W$  can be represented as a row-wise data structure in the vector form  $I = (I_1, \dots, I_n)$ , where  $I_i$  is the intensity of the *ith* pixel. Define  $P = (P_1, \dots, P_n)$ , where  $P_i$  is the coordinate position of the ith pixel. The two feature vectors of the U-Net outputs are the category label vector  $L = (L_1, \dots, L_n)$ and corresponding confidence vector  $F = (F_1, \dots, F_n)$ , where  $L_i \in C = \{c_1, c_2, \dots, c_{\tau} | c_j \in N, j = 1, \dots \}$  is a category label,  $\tau$  is the number of categories and  $0 \le F_i = F(L_i) \le 1$  is the confidence value of the *ith* pixel classified as  $L_i$ ,  $1 \le i \le \eta$ .

Suppose  $L^* = (L_1^*, \dots, L_n^*)$  is the actual category label vector of image I (ground truth),  $\tilde{L} = (\tilde{L}_1, \dots, \tilde{L}_n)$  is the predicted category label vector. For a certain type of  $c \in C$ , the Jaccard index is defined as:

$$J_{c}\left(L^{*}, \tilde{L}\right) = \frac{\left|\left\{i, 1 \leq i \leq \eta | L_{i}^{*} = c\right\} \cap \left\{i, 1 \leq i \leq \eta | \tilde{L}_{i} = c\right\}\right|}{\left|\left\{i, 1 \leq i \leq \eta | L_{i}^{*} = c\right\} \cup \left\{i, 1 \leq i \leq \eta | \tilde{L}_{i} = c\right\}\right|} (3)$$

where | is the number of elements in the set. Accordingly, Jaccard loss function is defined as:

$$\Delta_{J_c}(L^*, \check{L}) = 1 - J_c(L^*, \check{L}) \tag{4}$$

If the error prediction pixel set related to the category c is defined as:

$$M_c(L^*, \check{L}) = \left\{i, 1 \le i \le \eta | L_i^* = c, \tilde{L}_i \ne c\right\} \cup \left\{i, 1 \le i \le \eta | L_i^* \ne c, \tilde{L}_i = c\right\} (5)$$

Then, 
$$\Delta_{J_c}$$
 can be rewritten as,
$$\Delta_{J_c}(M_c) = \frac{|M_c|}{\left|\left\{i, 1 \le i \le \eta | L_i^* = c\right\} \cup M_c\right|}$$
(6)

The above loss function is defined at discrete points and cannot be minimized through a continuous optimization framework. In this paper, the Jaccard-Lovasz extension loss function was used in the same way as that proposed in the reference<sup>[20]</sup>, which is the Lovasz extension of the Jaccard loss function and is defined on a continuous interval,

$$\operatorname{loss}\left(L^{*}, \, \check{L}\right) = \frac{1}{|C|} \sum_{c \in C} \bar{\Delta}_{\operatorname{J}_{c}}(m(c)) \tag{7}$$

where  $c \in C$  is the category label, m(c) is the pixel labelling error vector corresponding to the c, defined as follows:

$$m(c) = (m_1(c), \dots, m_{\eta}(c))$$
 (8)

$$m_i(c) = \begin{cases} 1 - F_i(c) & \text{if } L_i^* = c \\ F_i(c), & \text{otherwise} \end{cases}$$
 (9)

and  $\bar{\Delta}_{J_c}$  is the Lovasz extension of the Jaccard loss function  $\Delta_{J_c}$ ,

$$\bar{\Delta}_{J_c}(m(c)) = \sum_{i=1}^{\eta} m_i g_i(m)$$
 (10)

$$g_i(m) = \Delta_{J_c}(\{\pi_1, \dots, \pi_i\}) - \Delta_{J_c}(\{\pi_1, \dots, \pi_{i-1}\})$$
 (11)

where  $(\pi_1, \dots, \pi_\eta)$  is a permutation ordering the components of m in descending order, i.e.  $m_{\pi_1} \ge m_{\pi_2} \ge \dots \ge m_{\pi_\eta}$ .

#### 3.3 CRF Post-processing

CRF (Conditional Random Field, CRF) <sup>[21]</sup> is an extension of the logistic regression classifier to arbitrary graphical structures. In this paper, CRF was used to finetune the classification results generated by the U-Net model for removing the blurred boundaries and obtaining a more accurate classification image.

The prediction category label  $L_i$  of the *ith* pixel can be considered as a random variable, and so the prediction category label vector  $L = (L_1, \dots, L_\eta)$  can be considered as a random field. For a given image  $I = (I_1, \dots, I_\eta)$ , the prediction category label can be considered as a condition random field with a distribution p(L|I).

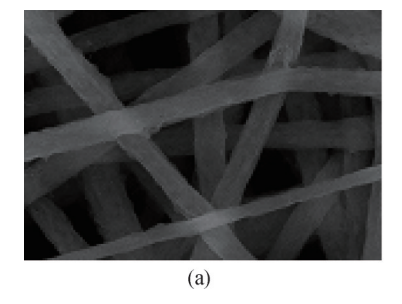
The CRF network uses the maximum likelihood method <sup>[22]</sup> as the loss function, which is defined by the energy functional,

$$E(L) = \sum_{i} \theta_{u}(L_{i}) + \sum_{i} \theta_{p}(L_{i}, L_{j})$$
 (12)

where  $\theta_u$  is a single-pixel energy defined as

$$\theta_u = -logF_i = -logF(L_i) \tag{13}$$

The greater the probability of classification



label  $F(L_i)$ , the smaller the penalty, indicating that the prediction is more accurate. Here,  $\theta_p$  is the energy of a pixel pair, which is defined as

$$\theta_p(L_i, L_j) = \mu(L_i, L_j)(\omega_1 k_1 + \omega_2 k_2)$$
 (14)

$$k_1 = \exp\left(-\frac{\|P_i - P_j\|^2}{2\sigma_\alpha^2} - \frac{\|I_i - I_j\|^2}{2\sigma_\beta^2}\right)$$
 (15)

$$k_2 = \exp\left(-\frac{\left\|P_i - P_j\right\|^2}{2\sigma_\gamma^2}\right) \tag{16}$$

where  $k_1, k_2$  are two Gaussian kernels defining the binary energy functional, and  $\omega_1$ ,  $\omega_2$  are the weights. The parameters  $\sigma_\alpha$ ,  $\sigma_\beta$ , and  $\sigma_\gamma$  are the standard deviations of the Gaussian kernels;  $P_i, P_j$  and  $I_i, I_j$  represent the location information and the pixel values of pixel i,j respectively.  $k_1$  tends to classify pixels with similar positions and similar pixel values as the same type of label;  $k_2$  can combine isolated points into the same labels as surrounding pixels which may increase the smoothness of the segmentation. Finally,  $\mu(L_i, L_j)$  represents a measurement of compatibility between two labels  $L_i$  and  $L_j$ . If the semantic categories represented by  $L_i$  and  $L_j$  are not compatible with each other, the corresponding value of  $\mu(L_i, L_j)$  is large which leads the large energy functional.

Fig. 3 consists of three parts in which (a) shows an original nanofiber SEM image, (b) with its U-Net segmentation result, and (c) the CRF post-processing results.

### 4 Numerical Experiments

#### 4.1 Data Set

The data set used in this study contains a total of 30 nanofiber SEM images, each with a resolution of  $714 \times 1024$  pixels in the data sets. Among them, 20 were used for training and the other 10 for testing. Given the small number of training images, each image in the data sets was divided into 35 overlapping blocks with the size of  $256 \times 256$ , contributing to a total of 700 blocks for training. Each training block required manual annotation. Fig. 4 shows an enlarged block of a SEM image and its corresponding manual labeling result.

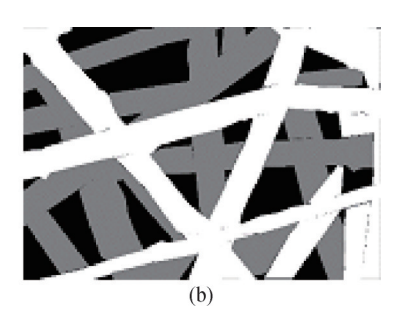


Fig. 4 Manual annotation: (a) A block of a nanofiber SEM image; (b) The manual labeling map of (a)

The experiments were performed on dual Intel Xeon E5-2620 v4 processors with dual NVIDIA Tesla P4 GPU, using the Python-OpenCV computer vision library for image processing and the PyTorch framework for network construction and training.

#### 4.2 Segmentation Results and Comparison

The hyper parameters used for the network training in this paper are shown in Table 1.

There are a total of three hyper parameters used in this work. Epoch means a complete training of the model

Table 1 Hyper parameters used for the network training

Hyper Parameter	Value
Epochs	20
Batch size	4
Learning rate	0.001

using all the data in the training set. Batch size means the number of samples selected for one training session. Learning rate means the speed of weight update.

Fig. 5 and Fig. 6 show one of the original SEM images used in the test and its segmentation results, respectively. The three segmentation results as shown in Fig. 6 were obtained using the U-Net multi-classifier, such that (a) shows the foreground, (b) the middle, and (c) the background.

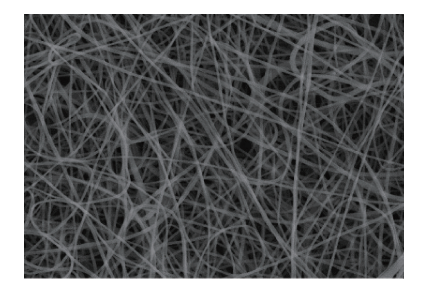
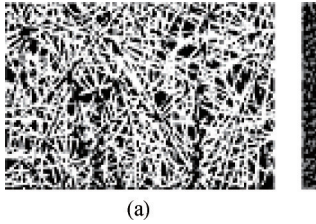
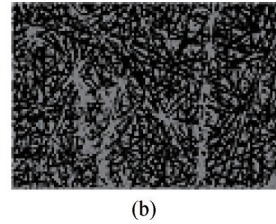


Fig.5 An original SEM image for test





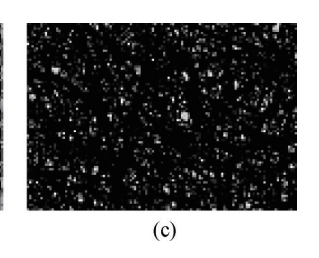


Fig. 6 The segmentation results of the original SEM image in Fig. 5: (a) The foreground mage; (b) The middle image; (c) The background image

In order to compare the results in Fig. 6 with the segmentation results by using the threshold method, a small block of the image from Fig. 5 is selected and shown in Fig.7.

Fig. 8 shows the segmentation results by using the threshold method and the U-Net multi-classifier in (a) and (b), respectively.

It can be seen that the segmentation results obtained by using the U-Net multi-classifier appear to have better details (white parts). This means that more detailed topology of nanofibers is retained and is beneficial to the extraction of the feature parameters.

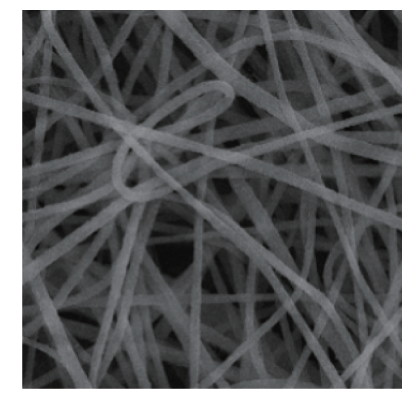
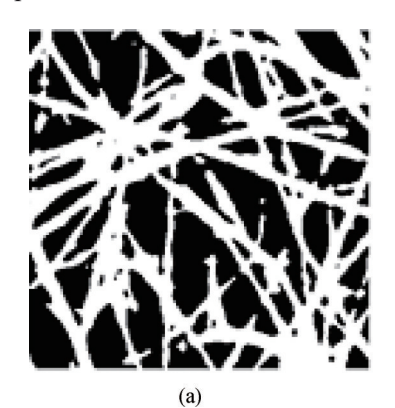


Fig.7 A small part extracted from Fig.5



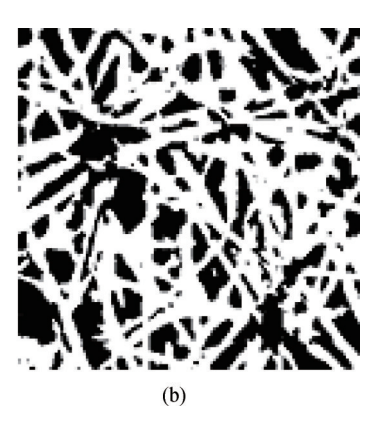


Fig. 8 Comparison of two segmentation methods: (a) Results obtained by the threshold segmentation; (b) Results obtained by the U-Net multi-classifier

# 5 Calculation of the Nanofiber Feature Parameters

In this section, two important feature parameters affecting the filtration performance were calculated based on the U-Net segmentation: porosity of a nanofiber filter membrane and the radius of the nanofibers.

#### 5.1 Porosity

The porosity of nanofiber filter membranes varies between 0 and 1 (or, as a percentage between 0% and 100%) and is defined as the fraction of volume of pores over the total volume in a nanofiber filter membrane,

$$\varepsilon = \frac{A_K}{A},\tag{17}$$

where  $\varepsilon$  is the porosity,  $A_K$  represents the area of the pores, A represents the area of the entire membrane image.

A nanofiber SEM image was partitioned into three images by using the U-Net multi-classifier: the foreground, the middle and the background. The background is the image obtained by removing the foreground and the middle from the original image, which is just the pore parts, as shown in the white parts of Fig. 6(c). The area of the white part can be calculated using the pixel numbers within it. On the other hand, the area of the entire image can be calculated using the pixel numbers of the entire image.

The porosities calculated from 10 testing SEM images range from 35.54% to 48.68%. For comparison, the actual values of the corresponding membranes were measured. The results shown in Table 2 indicate that the porosities calculated through segmented images are consistent with the measured values, although the former are generally smaller than the latter due to the loss of information caused by converting the 3D structure into a 2D structure.

Table 2	SEM	Image	Porosity
---------	-----	-------	----------

Ima	ge identification	Image1	Image2	Image3	Image4	Image5	Image6	Image7	Image8	Image9	Image10
Porosity	Calculated values	39.44%	48.68%	35.54%	41.98%	39.70%	37.28%	38.48%	43.62%	45.26%	40.89%
	Experimental values	41.91%	50.23%	37.13%	44.01%	41.59%	39.86%	39.98%	46.01%	47.14%	42.47%

#### 5.2 Nanofiber Radius

In the current study, only the radius of nanofibers located in the foreground were calculated. The medial axes of the nanofibers were extracted first by using morphological operators, and then the Circle function of

the OpenCV library<sup>[20]</sup> was used to detect the radius for every pixel point in the medial axes. Fig. 9 shows a small part of the medial axes of Fig. 6 (a).

Fig. 10 shows the sketch of the nanofiber radius detection, and Fig. 11 gives the radius distribution maps of Fig. 8 (a) and 8 (b) respectively.

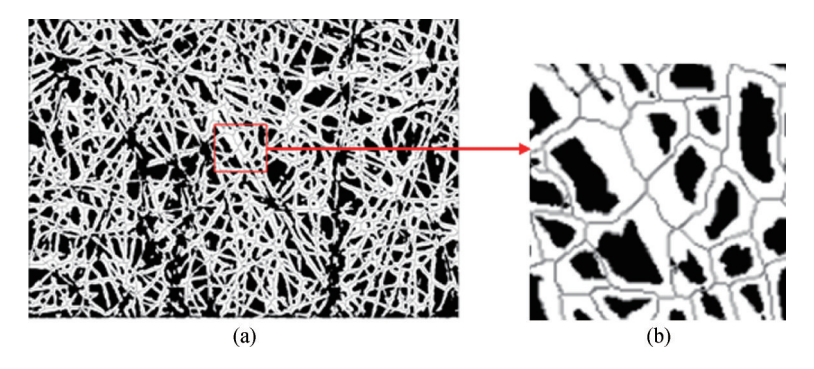


Fig. 9 Medial axes of Fig. 6(a): (a) The enlarged image of Fig. 6 (a); (b) Part of the medial axes

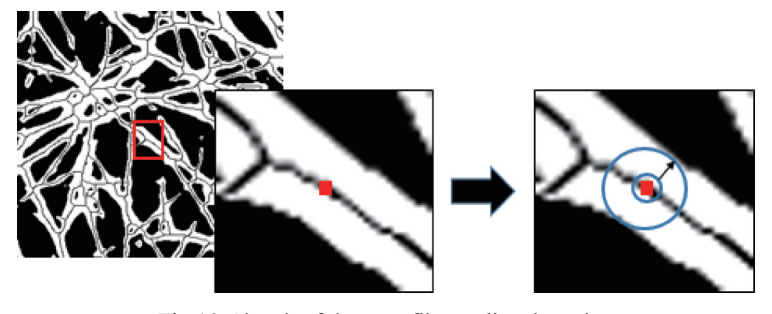
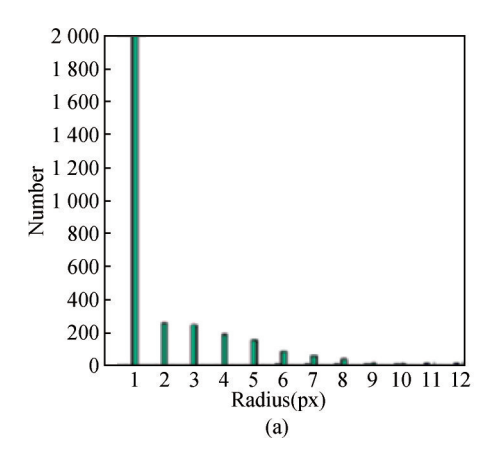


Fig.10 Sketch of the nanofiber radius detection



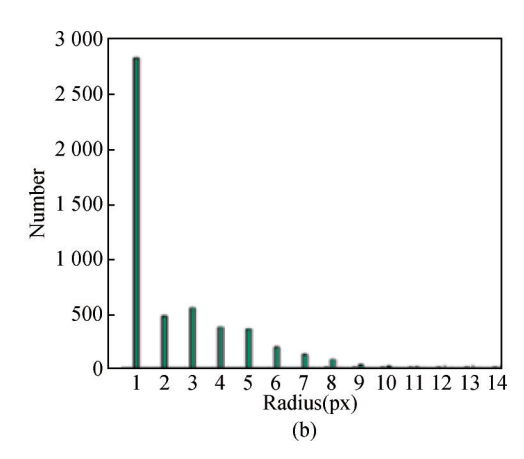


Fig.11 Nanofiber radius distribution maps: (a) The radius distribution map corresponding to the threshold segmentation; (b) The radius distribution map corresponding to the U-Net multi-classifier (foreground)

It can be seen that most of the nanofiber radii are distributed around one pixel, which means that the nanofibers are uniform, as illustrated in Fig. 7. There are 3054 pixels in the medial axes obtained by the threshold method and 5084 pixels obtained by U-Net multiclassifier. This means that the U-Net multiclassifier is able to retain better topological information of the nanofibers and is beneficial to the subsequent numerical simulation.

#### 6 Conclusion

In this paper, a U-Net multi-classifier was proposed. The U-Net network structure with the Jaccard-Lovasz extension loss function was used to classify the pixels of the nanofiber SEM image in three categories: the foreground, the middle and the background; and a CRF network was used to post-process the segmentation results. Two feature parameters, porosities of the filter membranes and the radius of the nanofibers, were calculated based on the segmentation Experimental results show that the segmentation obtained by the proposed U-Net multi-classifier can deal with overlapped nanofibers and retain more details of the SEM images. The proposed method is beneficial to the subsequent numerical simulation. Further research will be conducted to promote real-world industrial applications.

#### **Author Contribution:**

Conceptualization, Methodology and Supervision: Meiqing Wang, Fei Chen and Gaofeng Zheng; Data curation, Formal analysis and Investigation, Software: Zebin Chen; Funding acquisition: Gaofeng Zheng; Validation & Writing - original draf: Zebin Chen, Weiqi Gao; Writing - review & editing: Meiqing Wang, Choihong Lai and Shumin Guo.

#### **Acknowledgments:**

The authors wish to thank Olaf Ronneberger, Philipp Fischer, and Thomas Brox for sharing their code.

#### **Funding Information:**

This work was supported by the National Natural Science Foundation of China (52275575), and the Development and Reform Commission of Shenzhen Municipality (JSGG20220831094600002), Natural Science Foundation of Guangdong Province (2022A1515010923, 2022A1515010949).

#### **Data Availability:**

The authors declare that the main data supporting the findings of this study are available within the paper and its Supplementary Information files.

#### **Conflicts of Interest:**

The authors declare no competing interests.

#### Dates:

Received 09 January 2025; Accepted 17 July 2025; Published online 30 September 2025

#### Reference

- [1] M. N. Islam, B. Yıldırım, J. Maryska, F. Yalcınkaya, Journal of Industrial Textiles **2022**, 52, 152808372211274.
- [2] C. Lyu, P. Zhao, J. Xie, S. Dong, J. Liu, C. Rao, J. Fu, Nanomaterials (Basel) 2021, 11,
- [3] S. Divya, T. H. Oh, Polymers (Basel) 2022, 14,
- [4] Z. Shao, H. Chen, Q. Wang, G. Kang, X. Wang, W. Li, Y. Liu, G. Zheng, Separation and Purification Technology 2022, 302, 122175.
- [5] M. Parvinzadeh Gashti, S. A. Dehdast, A. Berenjian, M. Shabani, E. Zarinabadi, G. Chiari Fard, Gels 2023, 9,
- [6] A. Sharma, K. R. Sharma, J. M. Nunzi, A. Mahajan, P. D. Sharma, D. Pathak, Current Materials Science 2023, 16, 376.
- [7] M. Chu, Y. Diao, L. a. Zhang, J. Jiang, T. Mu, Journal of Engineered Fibers and Fabrics 2023, 18, 155892502211497.
- [8] H. Pujiarti, Z. A. Pangestu, N. Sholeha, N. Nasikhudin, M. Diantoro, J. Utomo, M. S. A. Aziz, Micromachines (Basel) 2023, 14,
- [9] C. W. Lou, M. C. Lin, C. H. Huang, M. F. Lai, B. C. Shiu, J. H.

- Lin, Polymers (Basel) 2022, 14,
- [10] Z. Sun, J. Shi, J. Wang, M. Jiang, Z. Wang, X. Bai, X. Wang, Nanoscale 2022, 14, 10761.
- [11] J. Qu, R. Wang, P. Pan, L. Du, Z. Mi, Y. Sun, X. Liu, IEEE Transactions on Automation Science and Engineering 2023, 20, 233.
- [12] Y. Lu, Y. Li, S. Zhang, G. Xu, K. Fu, H. Lee, X. Zhang, European Polymer Journal 2013, 49, 3834.
- [13] Y. Feng, R. Sun, M. Chen, C. Liu, Q. Wang, Journal of Applied Polymer Science **2017**, 135, 45653.
- [14] E. Shelhamer, J. Long, T. Darrell, IEEE Transactions on Pattern Analysis and Machine Intelligence **2017**, 39, 640.
- [15] H. Li, Y. Huang, Z. Zhang, IEEE Access 2017, 5, 13665.
- [16] K. He, G. Gkioxari, P. Dollár, R. Girshick, IEEE Transactions on Pattern Analysis & Machine Intelligence **2020**, 42, 386.
- [17] O. Ronneberger, P. Fischer, T. Brox. In Medical Image

- Computing and Computer-Assisted Intervention-MICCAI **2015**; Springer International Publishing, 2015, Chap. *Chapter* 28.
- [18] T. Eelbode, J. Bertels, M. Berman, D. Vandermeulen, F. Maes, R. Bisschops, M. B. Blaschko, IEEE Trans Med Imaging 2020, 39, 3679.
- [19] V. Badrinarayanan, A. Kendall, R. Cipolla, IEEE Transactions on Pattern Analysis and Machine Intelligence 2017, 39, 2481.
- [20] M. Berman, A. R. Triki, M. B. Blaschko, Ieee. 31st IEEE/CVF Conference on Computer Vision and Pattern Recognition (CVPR), Salt Lake City, UT, Jun 18-23 2018, pp 4413.
- [21] X. Glorot, A. Bordes, Y. Bengio, Journal of Machine Learning Research **2011**, 15, 315.
- [22] A. F. Vidal, V. De Bortoli, M. Pereyra, A. Durmus. IEEE International Conference on Image Processing (ICIP), 2019, pp 1742.